[CANCER RESEARCH 64, 4309–4318, June 15, 2004]

From the Cyclooxygenase-2 Inhibitor Celecoxib to a Novel Class of 3-Phosphoinositide-Dependent Protein Kinase-1 Inhibitors

Jiuxiang Zhu, Jui-Wen Huang, Ping-Hui Tseng, Ya-Ting Yang, Joseph Fowble, Chung-Wai Shiau, Yeng-Jeng Shaw, Samuel K. Kulp, and Ching-Shih Chen

Division of Medicinal Chemistry and Pharmacognosy, College of Pharmacy, The Ohio State University, Columbus, Ohio

ABSTRACT

The blockade of Akt activation through the inhibition of 3-phosphoinositide-dependent kinase-1 (PDK-1) represents a major signaling mechanism whereby celecoxib mediates apoptosis. Celecoxib, however, is a weak PDK-1 inhibitor (IC_{50}, 48 μM), requiring at least 30 μM to exhibit discernable effects on the growth of tumor cells *in vitro*. Here, we report the structure-based optimization of celecoxib to develop PDK-1 inhibitors with greater potency in enzyme inhibition and growth inhibition. Kinetics of PDK-1 inhibition by celecoxib with respect to ATP suggest that celecoxib derivatives inhibit PDK-1 by competing with ATP for binding, a mechanism reminiscent to that of many kinase inhibitors. Structure-activity analysis together with molecular modeling was used to generate compounds that were tested for their potency in inhibiting PDK-1 kinase activity and in inducing apoptosis in PC-3 prostate cancer cells. Docking of potent compounds into the ATP-binding site of PDK-1 was performed for lead optimization, leading to two compounds, OSU-03012 and OSU-03013, with IC_{50} values in PDK-1 inhibition and apoptosis induction in the low μM range. Exposure of PC-3 cells to these agents led to Akt dephosphorylation and inhibition of p70 S6 kinase activity. Moreover, overexpression of constitutively active forms of PDK-1 and Akt partially protected OSU-03012-induced apoptosis. Screening in a panel of 60 cell lines and more extensive testing in PC-3 cells indicated that the mean concentration for total growth inhibition was ~3 μM for both agents. Considering the conserved role of PDK-1/Akt signaling in promoting tumorigenesis, these celecoxib analogs are of translational relevance for cancer prevention and therapy.

INTRODUCTION

After demonstration of the efficacy of celecoxib in reducing colorectal polyps in patients with familial adenomatous polyposis (1), use of this cyclooxygenase (COX)-2 inhibitor in the prevention of epithelial malignancies has been the subject of a series of clinical trials. Despite these ongoing clinical investigations, the molecular mechanism underlying celecoxib-mediated *in vivo* antitumor effects remains elusive. At the cellular level, celecoxib inhibits COX-2 and causes cell cycle arrest and apoptosis in cancer cells. Evidence is accumulating that the *in vitro* effects of celecoxib on cell cycle progression and apoptosis are mediated through COX-2-independent signaling mechanisms (2–6). Among various putative pathways reported, the blockade of Akt activation through the inhibition of its upstream kinase, 3-phosphoinositide-dependent kinase-1 (PDK-1), is especially noteworthy (2–5, 7, 8). Our data indicate that celecoxib inhibits PDK-1/Akt signaling with moderate potency and that structural modifications allowed the inhibitory effect of celecoxib on Akt activation to be separated from the COX-2 inhibitory activity (4, 5). Together, this paradigm shift provides molecular underpinnings for the pharmacological exploitation of celecoxib to develop a novel class of potent PDK-1/Akt signaling inhibitors, of which the proof of principle has been demonstrated in our previous reports (4, 5).

The phosphatidylinositol 3′-kinase/PDK-1/Akt signaling cascade represents a convergence point for a plethora of receptor tyrosine kinase and cytokine-mediated pathways that regulate cell proliferation and survival and offers a framework to account for the ability of many extracellular trophic factors to maintain cell survival (9–15). Dysregulation of this signaling cascade due to constitutive growth factor-receptor activation and/or PTEN mutations results in Akt up-regulation, which subsequently promotes tumor invasiveness, angiogenesis, and progression (16–19). Thus, PDK-1/Akt signaling inhibitors are of translational relevance for development into useful chemotherapeutic or chemopreventive agents. In this study, we carried out structure-based optimization of celecoxib using an integrated approach combining structure-activity analysis and molecular modeling, leading to two potent PDK-1 inhibitors, OSU- 03012 and OSU-03013, with IC_{50} values at the low μM range. These two PDK-1 inhibitors could achieve total growth inhibition in 60 different human tumor cell lines at a mean concentration of ~3 μM.

MATERIALS AND METHODS

Reagents. Celecoxib was extracted from Celebrex capsules obtained from Amerisource Health (Malvern, PA) with ethyl acetate followed by recrystallization from a mixture of ethyl acetate and hexane. The Cell Death Detection ELISA kit was purchased from Roche Diagnostics (Mannheim, Germany). Rabbit polyclonal antibodies against Akt and phospho-^{473}Ser Akt were obtained from Cell Signaling Technologies (Beverly, MA). Mouse monoclonal anti-poly(ADP-ribose) polymerase (PARP) antibody was provided by PharMingen (San Diego, CA). The PDK-1 kinase assay kit was purchased from Upstate (Lake Placid, NY). Other chemical and biochemicals were obtained from Sigma-Aldrich (St. Louis, MO) unless otherwise mentioned. Nuclear magnetic resonance spectra (^{1}H NMR) were measured on Bruker 250 MHz. Chemical shifts (δ) are reported in parts per million relative to tetramethylsilane peak with $CDCl_3$ as solvent unless otherwise mentioned. High-resolution electrospray ionization mass spectrometry analyses were performed with a 3-Tesla Finnigan FTMS-2000 Fourier Transform mass spectrometer.

Synthesis of Chemicals. In this article, we discussed 36 compounds, of which the chemical names, proton nuclear magnetic resonance (^{1}H NMR), and high-resolution mass spectrometry data are summarized in Table 1. The procedures used to synthesize compounds 1–36 are described in the Supplementary Data section.

Cell Culture. PC-3 ($p53^{-/-}$) human androgen-nonresponsive prostate cancer cells were purchased from the American Type Tissue Collection (Manassas, VA). Cells were cultured in RPMI 1640 (Life Technologies, Inc., Grand Island, NY) supplemented with 10% fetal bovine serum (FBS; Life Technologies, Inc.) at 37°C in a humidified incubator containing 5% CO_2.

Cell Viability Analysis. The effect of celecoxib and its derivatives on PC-3 cell viability was assessed by using the 3-(4,5-dimethylthiazol-2-yl)-2,5-diphenyl-2*H*-tetrazolium bromide assay in six replicates. Cells were grown in 10% FBS- supplemented RPMI 1640 in 96-well, flat-bottomed plates for 24 h, and were exposed to various concentrations of celecoxib derivatives dissolved in DMSO (final concentration ≤0.1%) in 1% serum-containing RPMI 1640 for different time intervals. Controls received DMSO vehicle at a concentration equal to that in drug-treated cells. The medium was removed, replaced by 200

Received 12/29/03; revised 3/18/04; accepted 4/2/04.

Grant support: Public Health Service Grant CA94829 from National Cancer Institute, NIH, Department of Health and Human Services, and by Army Grant DAMD17-02-1-0117.

The costs of publication of this article were defrayed in part by the payment of page charges. This article must therefore be hereby marked *advertisement* in accordance with 18 U.S.C. Section 1734 solely to indicate this fact.

Note: Supplementary data for this article can be obtained from the corresponding author upon request.

Requests for reprints: Ching-Shih Chen, College of Pharmacy, The Ohio State University, 336 Parks Hall, 500 West 12th Avenue, Columbus, OH 43210-1291. Phone: (614) 688-4008; Fax: (614) 688-8556; E-mail: chen.844@osu.edu.

Table 1 *Nomenclatures, ^{1}H NMR,[a] and HRMS characterizations of compounds 1–36*

Compound	Description
1	4-[5-(4-(2-bromoethyl)phenyl)-3-(trifluoromethyl)-1*H*-pyrazol-1-yl]benzenesulfonamide ^{1}H-NMR δ 3.16 (t, *J* = 6.4, 2.0Hz, 2H), 3.60 (t, *J* = 6.4, 2.0 Hz, 2H), 4.90 (s, 2H), 6.75 (s, 1H), 7.13 (d, *J* = 8.0Hz, 2H), 7.20 (d, *J* = 8.0 Hz, 2H), 7.47 (d, *J* = 8.5Hz, 2H), 7.91 (d, *J* = 8.5Hz, 2H) $C_{18}H_{15}BrF_3N_3O_2S$; HRMS (M + Na^+): theoretical mass, 495.9913; actual mass, 495.9943
2	4-[5-(4-(3-bromopropyl)phenyl)-3-(trifluoromethyl)-1*H*-pyrazol-1-yl]benzenesulfonamide ^{1}H-NMR δ 2.16 (m, 2H), 2.81 (t, *J* = 7.1 Hz, 2H), 3.41 (t, *J* = 6.4 Hz, 2H), 5.08 (s, 2H), 6.76 (s, 1H), 7.15 (d, *J* = 8.2 Hz, 2H), 7.25 (d, *J* = 8.2 Hz, 2H), 7.47 (d, *J* = 8.5 Hz, 2H), 7.90 (d, *J* = 8.5 Hz, 2H) $C_{19}H_{17}BrF_3N_3O_2S$; HRMS (M + Na^+): theoretical mass, 510.0069; actual mass, 510.0042
3	4-[5-(4-(2-azidoethyl)phenyl)-3-(trifluoromethyl)-1*H*-pyrazol-1-yl]benzenesulfonamide ^{1}H-NMR δ 2.90 (t, *J* = 6.8 Hz, 2H), 3.51 (t, *J* = 6.8 Hz, 2H), 5.49 (s, 2H), 6.76 (s, 1H), 7.17 (d, *J* = 8.3 Hz, 2H), 7.24 (d, *J* = 8.3 Hz, 2H), 7.42 (d, *J* = 8.7 Hz, 2H), 7.85 (dd, *J* = 8.7, 2.0 Hz, 2H) $C_{18}H_{15}F_3N_6O_2S$; HRMS (M + Na^+): theoretical mass, 459.0821; actual mass, 459.0817
4	4-[5-(4-(3-azidopropyl)phenyl)-3-(trifluoromethyl)-1*H*-pyrazol-1-yl]benzenesulfonamide ^{1}H-NMR δ 1.83 (m, 2H), 2.64 (t, *J* = 7.5 Hz, 2H), 3.20 (t, *J* = 7.5 Hz, 2H), 5.31 (br s, 2H), 6.67 (s, 1H), 7.07 (m, 4H), 7.35 (dd, *J* = 7.5, 2.0 Hz, 2H), 7.79 (dd, *J* = 7.5, 2.0 Hz, 2H) $C_{19}H_{17}F_3N_6O_2S$; HRMS (M + Na^+): theoretical mass, 473.0978; actual mass, 473.0946
5	4-[5-(4-butylphenyl)-3-(trifluoromethyl)-1*H*-pyrazol-1-yl]benzenesulfonamide ^{1}H-NMR δ 0.93 (t, *J* = 7.2 Hz, 3H), 1.36 (m, 2H), 1.64 (m, 2H), 2.63 (t, *J* = 7.6 Hz, 2H), 5.54 (s, 2H), 6.76 (s, 1H), 7.15(d, *J* = 8.3 Hz, 2H), 7.20 (d, *J* = 8.3 Hz, 2H), 7.45 (dt, *J* = 8.8, 2.0 Hz, 2H), 7.88 (dt, *J* = 8.8, 2.0 Hz, 2H) $C_{20}H_{20}F_3N_3O_2S$; HRMS (M + Na^+): theoretical mass, 446.1120; actual mass, 446.1149
6	4-[5-(4-t-butylphenyl)-3-(trifluoromethyl)-1*H*-pyrazol-1-yl]benzenesulfonamide ^{1}H-NMR δ 1.33 (s, 9H), 4.90 (s, 2H), 6.53 (s, 1H), 7.32 (dd, *J* = 9.7 Hz, 4H), 7.42 (d, *J* = 8.8 Hz, 2H), 8.02 (d, *J* = 8.8 Hz, 2H) $C_{20}H_{20}F_3N_3O_2S$; HRMS (M + Na^+): theoretical mass, 446.1120; actual mass, 446.1118
7	4-[5-(2-naphthalenyl)-3-(trifluoromethyl)-1*H*-pyrazol-1-yl]benzenesulfonamide ^{1}H-NMR δ 5.47 (s, 2H), 6.89 (s, 1H), 7.18 (dd, *J* = 8.6, 1.6 Hz, 1H), 7.42 (bd, *J* = 8.6 Hz, 2H), 7.51–7.55 (m, 2H), 7.78–7.83 (m, 6H) $C_{20}H_{14}F_3N_3O_2S$; HRMS (M + Na^+): theoretical mass, 440.0651; actual mass, 440.0657
8	4-[5-(3-indolyl)-3-(trifluoromethyl)-1*H*-pyrazol-1-yl]benzenesulfonamide ^{1}H-NMR δ(acetone-d_6) 6.69 (br s, 1H), 7.03–7.08 (m, 2H), 7.19 (t, *J* = 7.2 Hz, 1H), 7.40 (d, *J* = 7.8 Hz, 1H), 7.50 (d, *J* = 7.8 Hz, 1H), 7.67 (d, *J* = 8.7 Hz, 2H), 7.92 (d, *J* = 8.7 Hz, 2H) $C_{18}H_{13}F_3N_4O_2S$; HRMS (M + Na^+): theoretical mass, 429.0603; actual mass, 429.0606
9	4-[5-(4-biphenylyl)-3-(trifluoromethyl)-1*H*-pyrazol-1-yl]benzenesulfonamide ^{1}H-NMR δ 4.81(s, 2H), 6.75 (s, 1H), 7.23 (d, *J* = 8.5 Hz, 2H), 7.34–7.56 (m, 5H), 7.56 (m, 4H), 7.86 (d, *J* = 8.5 Hz, 2H) $C_{22}H_{16}F_3N_3O_2S$; HRMS (M + Na^+): theoretical mass, 466.0807; actual mass, 466.0811
10	4-[5-(4'-chloro[1,1'-biphenyl]-4-yl)-3-(trifluoromethyl)-1*H*-pyrazol-1-yl]benzenesulfonamide ^{1}H-NMR δ 5.42 (s, 2H), 6.83 (s, 1H), 7.30 (d, *J* = 8.2 Hz, 2H), 7.40–7.59 (m, 8H), 7.92 (d, *J* = 8.2 Hz, 2H) $C_{22}H_{15}ClF_3N_3O_2S$; HRMS (M + Na^+): theoretical mass, 500.0418; actual mass, 500.0432
11	4-[5-(3',5'-dichloro[1,1'-biphenyl]-4-yl)-3-(trifluoromethyl)-1*H*-pyrazol-1-yl]benzenesulfonamide ^{1}H-NMR δ 4.85 (s, 2H), 6.82 (s, 1H), 7.30 (d, *J* = 8.8 Hz, 2H), 7.36 (s, 1H), 7.37–7.57 (m, 6H), 7.93 (d, *J* = 8.8 Hz, 2H) $C_{22}H_{14}Cl_2F_3N_3O_2S$; HRMS (M + Na^+): theoretical mass, 534.0028; actual mass, 534.0016
12	4-[5-(2',3'-dichloro[1,1'-biphenyl]-4-yl)-3-(trifluoromethyl)-1*H*-pyrazol-1-yl]benzenesulfonamide ^{1}H-NMR δ 4.85 (s, 2H), 6.76 (s, 1H), 7.18–7.25 (m, 3H), 7.35–7.49 (m, 6H), 7.88 (d, *J* = 8.6 Hz, 2H) $C_{22}H_{14}Cl_2F_3N_3O_2S$; HRMS (M + Na^+): theoretical mass, 534.0028; actual mass, 533.9999
13	4-[5-(2',4',5'-trichloro[1,1'-biphenyl]-4-yl)-3-(trifluoromethyl)-1*H*-pyrazol-1-yl]benzenesulfonamide ^{1}H-NMR δ 4.86 (s, 2H), 6.77 (s, 1H), 7.25 (dt, *J* = 8.6, 2.0 Hz, 2H), 7.37 (dt, *J* = 8.6, 2.0 Hz, 2H), 7.39 (s, 1H), 7.46 (dt, *J* = 8.8, 2.0 Hz, 2H), 7.54 (s, 1H), 7.88 (dt, *J* = 8.9, 1.2 Hz, 2H) $C_{22}H_{13}Cl_3F_3N_3O_2S$; HRMS (M + Na^+): theoretical mass, 567.9638; actual mass, 567.9679
14	4-[5-(4'-methyl[1,1'-biphenyl]-4-yl)-3-(trifluoromethyl)-1*H*-pyrazol-1-yl]benzenesulfonamide ^{1}H-NMR δ 2.32 (s, 3H), 4.75 (s, 2H), 6.72 (s, 1H), 7.18–7.21 (m, 4H), 7.39–7.52 (m, 6H), 7.84 (d, *J* = 8.9 Hz, 2H) $C_{23}H_{18}F_3N_3O_2S$; HRMS (M + Na^+): theoretical mass, 480.0964; actual mass, 480.0961
15	4-[5-(4'-trifluoromethyl[1,1'-biphenyl]-4-yl)-3-(trifluoromethyl)-1*H*-pyrazol-1-yl]benzenesulfonamide ^{1}H-NMR δ 5.19 (s, 2H), 6.86 (s, 1H), 7.36 (d, *J* = 8.0 Hz, 2H), 7.53 (d, *J* = 8.5 Hz, 2H), 7.65 (m, 6H), 7.92 (d, *J* = 8.5 Hz, 2H) $C_{23}H_{15}F_6N_3O_2S$; HRMS (M + Na^+): theoretical mass, 534.0681; actual mass, 534.0677
16	4-[5-(4'-bromomethyl[1,1'-biphenyl]-4-yl)-3-(trifluoromethyl)-1*H*-pyrazol-1-yl]benzenesulfonamide ^{1}H-NMR δ 3.92 (s, 2H), 4.93 (s, 2H), 6.66 (s, 1H), 7.03–7.26 (m, 8H), 7.38 (d, *J* = 8.6 Hz, 2H), 7.82 (d, *J* = 8.6 Hz, 2H) $C_{23}H_{17}BrF_3N_3O_2S$; HRMS (M + Na^+): theoretical mass, 558.0069; actual mass, 558.0112
17	4-[5-(3',5'-dimethyl[1,1'-biphenyl]-4-yl)-3-(trifluoromethyl)-1*H*-pyrazol-1-yl]benzenesulfonamide ^{1}H-NMR δ 2.40 (s, 6H), 5.38 (br s, 2H), 6.83 (s, 1H), 7.05 (s, 1H), 7.25 (m, 4H), 7.50 (dd, *J* = 6.7, 1.7 Hz, 2H), 7.59 (dd, *J* = 6.7, 1.7 Hz, 2H), 7.92 (dd, *J* = 6.7, 1.7 Hz, 2H) $C_{24}H_{20}F_3N_3O_2S$; HRMS (M + Na^+): theoretical mass, 494.1120; actual mass, 494.1119
18	4-[5-(4'-butyl[1,1'-biphenyl]-4-yl)-3-(trifluoromethyl)-1*H*-pyrazol-1-yl]benzenesulfonamide ^{1}H-NMR δ 0.96 (t, *J* = 7.5 Hz, 3H), 1.41 (m, 2H), 1.66 (m, 2H), 2.68 (t, *J* = 7.5 Hz, 2H), 5.20 (br s, 2H), 6.84 (s, 1H), 7.29 (dd, *J* = 8.2, 2.0 Hz, 4H), 7.53 (dt, *J* = 8.2, 2.0 Hz, 4H), 7.62 (d, *J* = 8.5 Hz, 2H), 7.93 (d, *J* = 8.5 Hz, 2H) $C_{26}H_{24}F_3N_3O_2S$; HRMS (M + Na^+): theoretical mass, 522.1433; actual mass, 522.1466
19	4-[5-(4'-*tert*-butyl[1,1'-biphenyl]-4-yl)-3-(trifluoromethyl)-1*H*-pyrazol-1-yl]benzenesulfonamide ^{1}H-NMR δ 1.35 (s, 9H), 4.87 (s, 2H), 6.59 (s, 1H), 7.44–7.57 (m, 6H), 7.58 (d, *J* = 7.5 Hz, 2H), 7.92 (d, *J* = 8.7 Hz, 2H), 8.12 (d, *J* = 7.5 Hz, 2H) $C_{26}H_{24}F_3N_3O_2S$; HRMS (M + Na^+): theoretical mass, 522.1433; actual mass, 522.1401
20	4-[5-(4-(phenylmethyl)phenyl)-3-(trifluoromethyl)-1*H*-pyrazol-1-yl]benzenesulfonamide ^{1}H-NMR δ 3.71 (s, 2H), 4.74 (s, 2H), 6.52 (s, 1H), 6.91–7.11 (m, 9H), 7.27 (d, *J* = 8.9 Hz, 2H), 7.69 (d, *J* = 8.9 Hz, 2H) $C_{23}H_{18}F_3N_3O_2S$; HRMS (M + Na^+): theoretical mass, 480.0964; actual mass, 480.0938
21	4-[5-(9H-fluoren-2-yl)-3-(trifluoromethyl)-1*H*-pyrazol-1-yl]benzenesulfonamide ^{1}H-NMR δ 3.88 (s, 2H), 4.64 (s, 2H), 6.68 (s, 1H), 7.26–7.38 (m, 4H), 7.56 (d, *J* = 8.7 Hz, 2H), 7.74–7.81 (m, 3H), 7.90 (d, *J* = 8.7 Hz, 2H) $C_{23}H_{16}F_3N_3O_2S$; HRMS (M + Na^+): theoretical mass, 478.0807; actual mass, 478.0771
22	4-[5-(9-anthracenyl)-3-(trifluoromethyl)-1*H*-pyrazol-1-yl]benzenesulfonamide ^{1}H-NMR δ 4.63 (s, 2H), 6.93 (s, 1H), 7.33 (d, *J* = 6.8 Hz, 2H), 7.45–7.55 (m, 8H), 8.04 (d, *J* = 6.8 Hz, 2H), 8.60 (s, 1H) $C_{24}H_{16}F_3N_3O_2S$; HRMS (M + Na^+): theoretical mass, 490.0807; actual mass, 490.0769
23	4-[5-(2-phenanthrenyl)-3-(trifluoromethyl)-1*H*-pyrazol-1-yl]benzenesulfonamide ^{1}H-NMR δ (600 MHz) 4.89 (s, 2H), 6.92 (s, 1H), 7.37 (dd, *J* = 8.5, 1.4 Hz, 1H), 7.51 (d, *J* = 8.6 Hz, 2H), 7.65–7.69 (m, 3H), 7.80 (d, *J* = 8.8 Hz, 1H), 7.86–7.92 (m, 4H), 8.64 (d, *J* = 8.4 Hz, 2H) $C_{24}H_{16}F_3N_3O_2S$; HRMS (M + Na^+): theoretical mass, 490.0807; actual mass, 490.0805
24	4-[5-(9-phenanthrenyl)-3-(trifluoromethyl)-1*H*-pyrazol-1-yl]benzenesulfonamide ^{1}H-NMR δ 4.76 (s, 2H), 6.90 (s, 1H), 7.43–7.84 (m, 11H), 8.72 (t, *J* = 7.8 Hz, 2H) $C_{24}H_{16}F_3N_3O_2S$; HRMS (M + Na^+): theoretical mass, 490.0807; actual mass, 490.0833

Table 1 *Continued*

Compound	Description
25	4-[5-(2-phenanthrenyl)-3-(trifluoromethyl)-1*H*-pyrazol-1-yl] benzenecarboxamide ^{1}H-NMR δ 5.75–6.05 (br d, 2H), 7.0 (s, 1H), 7.50 (dd, *J* = 8.5, 1.4 Hz, 1H), 7.55 (d, *J* = 8.5 Hz, 2H), 7.77 (m, 3H), 7.88 (m, 3H), 7.90 (m, 2H), 8.72 (m, 2H) $C_{25}H_{16}F_3N_3O$; HRMS (M + Na^+): theoretical mass, 454.0038; actual mass, 454.1142
26	4-[5-(2-phenanthrenyl)-3-(trifluoromethyl)-1*H*-pyrazol-1-yl]-benzonitrile ^{1}H-NMR δ 6.91(s, 1H), 7.46 (s, 1H), 7.50 (d, *J* = 2.0 Hz, 2H), 7.63–7.79 (m, 5H), 7.83 (d, *J* = 2.0 Hz, 2H), 7.92 (m, 1H), 8.64 (d, *J* = 8.4 Hz, 2H) $C_{25}H_{14}F_3N_3$; HRMS (M + Na^+): theoretical mass, 436.1032; actual mass, 436.1032
27	4-[5-(2-phenanthrenyl)-3-(trifluoromethyl)-1*H*-pyrazol-1-yl]-N-hydroxy-benzamidine ^{1}H-NMR δ 7.10 (s, 1H), 7.34 (dd, *J* = 4.0, 0.9 Hz, 1H), 7.36 (d, *J* = 0.9 Hz, 1H), 7.37 (d, *J* = 0.9 Hz, 1H), 7.42–7.45 (m, 3H), 7.46 (d, *J* = 0.8 Hz, 1H), 7.51–7.52 (m, 2H), 7.53 (d, *J* = 0.9 Hz, 1H), 7.57 (s, 1H), 7.89 (s, 1H), 7.91 (s, 1H) $C_{25}H_{17}F_3N_3O$; HRMS (M + Na^+): theoretical mass, 469.1220; actual mass, 469.1247
28	5-(2-phenanthrenyl)-3-(trifluoromethyl)-4-(1*H*-tetrazol-5-ylphenyl)-1*H*-pyrazole ^{1}H-NMR δ 6.82 (s, 1H), 7.28 (d, *J* = 1.8 Hz, 1H), 7.38 (d, *J* = 8.7 Hz, 2H), 7.48–7.74 (m, 5H), 7.74 (d, *J* = 2.5 Hz, 2H), 7.95 (d, *J* = 8.7 Hz, 2H), 8.47 (d, *J* = 8.7 Hz, 2H) $C_{25}H_{15}F_3N_6$; HRMS (M + Na^+): theoretical mass, 479.1202; actual mass, 479.1225
29	4-[5-(2-phenanthrenyl)-3-(trifluoromethyl)-1*H*-pyrazol-1-yl]-benzaldehyde oxime ^{1}H-NMR δ 6.81 (s, 1H), 7.27–7.30 (m, 3H), 7.47 (d, *J* = 8.7 Hz, 2H), 7.52–7.57 (m, 4H), 7.68 (d, *J* = 8.8 Hz, 2H), 7.75–7.79 (m, 2H), 8.48–8.53 (m, 2H) $C_{25}H_{16}F_3N_3O$; HRMS (M + Na^+): theoretical mass, 454.1137; actual mass, 454.1106
30	4-[5-(2-phenanthrenyl)-3-(trifluoromethyl)-1*H*-pyrazol-1-yl]-benzaldehyde hydrazone ^{1}H-NMR δ 6.81 (s, 1H), 7.27–7.30 (m, 2H), 7.33 (d, *J* = 1.8 Hz, 1H), 7.42 (d, *J* = 8.6 Hz, 1H), 7.53–7,55 (m, 2H), 7.57–7.60 (m, 2H), 7.68 (d, *J* = 8.9 Hz, 2H), 7.75 (d, *J* = 1.7 Hz, 1H), 7.80 (s, 1H), 8.48–8.55 (m, 2H) $C_{25}H_{17}F_3N_4$; HRMS (M + Na^+): theoretical mass, 453.1297; actual mass, 453.1302
31	{4-[5-(2-phenanthrenyl)-3-(trifluoromethyl)-1*H*-pyrazol-1-yl]-phenyl}-acetonitrile ^{1}H-NMR δ 3.77 (s, 2H), 6.93 (s, 1H), 7.29–7.43 (m, 4H), 7.66–7.86 (m, 6H), 8.65 (t, *J* = 7.0 Hz, 3H) $C_{26}H_{16}F_3N_3$; HRMS (M + Na^+): theoretical mass, 450.1151; actual mass, 450.1188
32	2-{4-[5-(2-phenanthrenyl)-3-(trifluoromethyl)-1*H*-pyrazol-1-yl]-phenyl}-N-hydroxy-acetamidine ^{1}H-NMR δ 3.30 (s, 1H), 3.38 (s, 1H), 6.83 (s, 1H), 7.20–7.41 (m, 4H), 7.59–7.89 (m, 6H), 8.55–8.60 (m, 3H) $C_{26}H_{19}F_3N_4O$; HRMS (M + Na^+): theoretical mass, 461.1580; actual mass, 461.1584
33	5-(2-phenanthrenyl)-3-(trifluoromethyl)-4-(1*H*-tetrazol-5-ylmethylphenyl)-1*H*-pyrazole ^{1}H-NMR δ 4.45 (s, 2H). 7.15 (s, 1H), 7.42 (s, 4H), 7.53 (d, *J* = 6.9 Hz, 1H), 7.66–7.76 (m, 3H), 7.89 (d, *J* = 7.2 Hz, 1H), 8.01 (m, 2H), 8.78 (t, *J* = 6.9 Hz, 2H) $C_{26}H_{17}F_3N_6$; HRMS (M + Na^+): theoretical mass, 493.1335; actual mass, 493.1359
34	2-amino-N-{4-[5-(2-phenanthrenyl)-3-(trifluoromethyl)-1*H*-pyrazol-1-yl]-phenyl} acetamide ^{1}H-NMR δ 3.48 (s, 2H), 6.92 (s, 1H), 7.35 (d, *J* = 8.8 Hz, 2H), 7.42 (dd, *J* = 8.6, 1.7 Hz, 1H), 7.62–7.72 (m, 5H), 7.79 (d, *J* = 8.8 Hz, 1H), 7.85–7.94 (m, 2H), 8.62 (t, *J* = 8.5 Hz, 2H), 9.56 (br s, 1H) $C_{26}H_{19}F_3N_4O$; HRMS (M + Na^+): theoretical mass, 483.1403; actual mass, 483.1389
35	4-[5-(2-phenanthrenyl)-3-(trifluoromethyl)-1*H*-pyrazol-1-yl]-phenyl-guanidine ^{1}H-NMR δ 6.90 (s, 1H), 7.19 (d, *J* = 8.7 Hz, 2H), 7.34 (dd, *J* = 8.7, 2.0 Hz, 1H), 7.39 (d, *J* = 8.7 Hz, 2H), 7.61–7.67 (m, 3H), 7.79 (d, *J* = 9.0 Hz, 1H), 7.84–7.91 (m, 3H), 8.62 (d, *J* = 8.3 Hz, 2H), 9.95(s, 1H) $C_{25}H_{18}F_3N_5$; HRMS (M + H^+): theoretical mass, 446.1587(M+H); actual mass, 446.1596(M+H)
36	2-{4-[5-(2-phenanthrenyl)-3-(trifluoromethyl)-1*H*-pyrazol-1-yl]-phenylamino}-acetamide ^{1}H-NMR δ(DMSO-d_6) 3.61 (d, *J* = 6.0 Hz, 2H), 6.28 (br t, *J* = 6.0 Hz, 1H), 6.55 (d, *J* = 8.8 Hz, 2H), 7.10 (br s, 1H), 7.13 (d, *J* = 8.8 Hz, 2H), 7.29 (s, 1H), 7.38 (br s, 1H), 7.44–7.48 (dd, *J* = 8.7, 1.9 Hz, 1H), 7.66–7.71 (m, 2H), 7.75–7.91 (m, 2H), 8.01 (m, 1H), 8.07 (d, *J* = 1.9 Hz, 1H), 8.81 (m, 2H) $C_{26}H_{19}F_3N_4O$; HRMS (M + Na^+): theoretical mass, 483.1403; actual mass, 483.1415
37	4-[5-(2-phenanthrenyl)-3-(trifluoromethyl)-1*H*-pyrazol-1-yl]-phenyl-urea ^{1}H-NMR δ 6.98 (s, 1H), 7.19 (dt, *J* = 8.9, 2.1 Hz, 2H), 7.34–7.42 (m, 3H), 7.51–7.62 (m, 4H), 7.70 (d, *J* = 9.0 Hz, 1H), 7.81–7.85 (m, 2H), 8.59–8.64 (m, 2H) $C_{25}H_{17}F_3N_4O$; HRMS (M + Na^+): theoretical mass, 469.1252; actual mass, 469.1199

[a] ^{1}H NMR, proton nuclear magnetic resonance; HRMS, high resolution mass spectrometry.

μl of 0.5 mg/ml of 3-(4,5-dimethylthiazol-2-yl)-2,5-diphenyl-2*H*-tetrazolium bromide in 10% FBS-containing RPMI 1640, and cells were incubated in the CO_2 incubator at 37°C for 2 h. Supernatants were removed from the wells, and the reduced 3-(4,5-dimethylthiazol-2-yl)-2,5-diphenyl-2*H*-tetrazolium bromide dye was solubilized in 200 μl/well DMSO. Absorbance at 570 nm was determined on a plate reader.

Cell Proliferation. PC-3 cells were seeded into six-well plates at ~75,000 cells/well in 10% FBS-containing RPMI 1640. After a 24-h attachment period, cells were treated in triplicate with the indicated concentration of celecoxib derivatives or DMSO vehicle in 10% FBS-containing RPMI 1640. At different time intervals, cells were harvested by trypsinization and numerated using a Coulter counter model Z1 D/T (Beckman Coulter, Fullerton, CA).

Apoptosis Analysis. Two methods were used to assess drug-induced apoptotic cell death: detection of DNA fragmentation by the Cell Death Detection ELISA kit (Roche Diagnostics) and Western blot analysis of PARP cleavage. The ELISA was performed according to the manufacturer's instructions and is based on the quantitative determination of cytoplasmic histone-associated DNA fragments in the form of mononucleosomes or oligonucleosomes generated after induced apoptotic death. In brief, 4×10^5 PC-3 cells were cultured in a T-25 flask for 24 h before treatment. Cells were treated with the DMSO vehicle or the test agent at the indicated concentrations for 6–24 h, collected, and cell lysates equivalent to 2×10^3 PC-3 cells were used in the ELISA. For the PARP cleavage assay, drug-treated cells were collected 4–8 h after treatment, washed with ice-cold PBS, and resuspended in lysis buffer containing 20 mM Tris-HCl (pH 8.0), 137 mM NaCl, 1 mM $CaCl_2$, 10% glycerol, 1% NP40, 0.5% deoxycholate, 0.1% SDS, 100 μM 4-(2-aminoethyl)-benzenesulfonyl fluoride, leupeptin at 10 μg/ml, and aprotinin at 10 μg/ml. Soluble cell lysates were collected after centrifugation at 10,000 × *g* for 5 min. Equivalent amounts of proteins (60–100 μg) from each lysate were resolved in 8% SDS- polyacrylamide gels. Bands were transferred to nitrocellulose membranes and analyzed by immunoblotting with anti-PARP antibody.

Immunoblotting. The general procedure for the Western blot analysis of Akt and phospho-Akt is described as follows. Cells were washed in PBS, resuspended in SDS sample buffer, sonicated by an ultrasonic sonicator for 5 s, and boiled for 5 min. After brief centrifugation, equivalent protein concentrations from the soluble fractions were resolved in 10% SDS-polyacrylamide gels on a Minigel apparatus, and transferred to a nitrocellulose membrane using a semi-dry transfer cell. The transblotted membrane was washed three times with TBS containing 0.05% Tween 20 (TBST). After blocking with TBST containing 5% nonfat milk for 60 min, the membrane was incubated with the primary antibody at 1:1000 dilution in TBST-5% low fat milk at 4°C for 12 h, and was then washed three times with TBST. The membrane was probed with goat antirabbit IgG-horseradish peroxidase conjugates (1:1000) for 1 h at room temperature and was washed with TBST three times. The immunoblots were visualized by enhanced chemiluminescence.

PDK-1 Kinase Assay. This *in vitro* assay was performed using a PDK-1 kinase assay kit (Upstate) according to the vendor's instructions. This cell-free assay is based on the ability of recombinant PDK-1, in the presence of DMSO vehicle or the test agent, to activate its downstream kinase serum- and glucocorticoid-regulated kinase which, in turn, phosphorylates the Akt/serum- and glucocorticoid-regulated kinase-specific peptide substrate RPRAATF with [γ-^{32}P]ATP. The ^{32}P-phosphorylated peptide substrate was then separated from the residual [γ-^{32}P]-ATP using P81 phosphocellulose paper and quantitated by a scintillation counter after three washes with 0.75% phosphoric acid. The reported values represent the means of two independent determinations.

Immunoprecipitated Akt Kinase Assay. Akt immunoprecipitation was carried out according to a modified, published procedure (7). PC-3 cells were treated with DMSO vehicle or the test agents at the indicated concentrations for 2 h and then lysed at 4°C for 1 h in buffer A containing 50 mM Tris-HCl (pH 7.5), 1% Triton X-100, 1 mM EDTA, 1 mM EGTA, 50 mM sodium fluoride, 10 mM sodium β-glycerophosphate, 0.1% 2-mercaptoethanol, 0.1 mM phenylmethylsulfonyl fluoride, and 1 μg/ml each of aprotinin, pepstatin, and leupeptin. Cell lysates were centrifuged at 10,000 $\times$ *g* for 5 min, and the supernatant was treated with anti-Akt at 4°C for 60 min, followed by protein G-agarose beads for additional 60 min. The immunoprecipitate was used to analyze Akt kinase activity by using the Akt/serum- and glucocorticoid-regulated kinase-specific peptide substrate RPRAATF as described above. Values represent the means of two independent determinations.

Immunoprecipitated p70 S6 kinase (p70^{S6K}) Assay. Immunoprecipitation of p70^{S6K} was carried out according to a modification of a published procedure (20). In brief, PC-3 cells were cultured in T-75 flasks (1.5×10^6/flask), and treated with OSU-03012 at the indicated concentrations in 1% FBS-containing RPMI 1640 for 6 h. Both floating and adherent cells were collected and lysed in 1 ml of lysis buffer [50 mM Tris (pH7.4), 150 mM NaCl, 1% NP40, 0.5% sodium deoxycholate, 1 mM EGTA, and 10% protease inhibitor mixture (Calbiochem)] for 30 min on ice. Lysates were centrifuged at 10,000 $\times$ *g* at 4°C for 20 min. Equal amounts of total protein were subject to immunoprecipitation with anti-p70^{S6K} antibody (sc-8418; Santa Cruz Biotechnology, Santa Cruz, CA). The mixture was incubated on ice with rocking for 1 h, followed by incubation with protein A-Sepharose bead for 2 h. The immunocomplex was washed with lysis buffer twice, followed by assay buffer [20 mM 4-morpholinepropanesulfonic acid (pH 7.2), 25 mM β-glycerol phosphate, 5 mM EGTA, 1 mM sodium orthovanadate, and 1 mM DTT], and resuspended in assay buffer. The assay was carried out using a p70^{S6K} assay kit (Upstate) according to the manufacturer's instruction.

Transient Transfection. The constitutively active Akt construct HA-PKBT308D/S473D and the constitutively active PDK-1 construct pcDNA-PDK1-A280V were kindly provided by Dr. Brain Hemmings (Friedrich Miescher Institute, Basel, Switzerland) and Dr. Feng Liu (University of Texas Health Science Center, San Antonio, TX), respectively. PC-3 cells were seeded into T-75 flasks (1.5×10^6/flask). Aliquots containing 3 μg of each plasmid or a control pcDNA3.1(+) vector in 750 μl of Opti-MEM (Invitrogen-Life Technologies, Inc.) were incubated with 9 μl of the FuGene 6 reagent (Roche Diagnostics Corp., Indianapolis, IN) for 15 min. Each flask was washed with Opti-MEM and then received the plasmid-FuGene 6 mixture and 4 ml of Opti-MEM. The flask was placed in a CO_2 incubator for 4 h, and the transfection medium was replaced with 10% FBS-supplemented RPMI 1640. After 24 h, Mock-, Akt-, and PDK-1-transfected PC-3 cells were seeded into 96-well plates at 5000 cells/well in 10% FBS-supplemented RPMI 1640. On the next day, cells were treated in four replicates with the indicated concentrations of OSU-03012 in 1% FBS- containing medium for 24 h. 3-(4,5-Dimethylthiazol-2-yl)-2,5-diphenyl-2*H*-tetrazolium bromide assay was used to determine the cell viability.

Molecular Modeling. The crystal structure of PDK-1 in complex with ATP, obtained from the Brookhaven Protein Data Bank (entry code 1H1W), was subject to the deletion of heteroatoms and the addition of polar hydrogens, partial atomic charges, and atomic solvation parameters using the molecular modeling software AutoDock Tools.[1] The three-dimensional structures of small molecules were generated using the software SYBYL 6.9 (Tripos Associate, St. Louis, MO; 2002). Gasteiger charges were computed, and energy minimization was carried out with default parameters. AutoDock Tools software was used to designate the rotable bonds and generate grid parameter file and docking parameter file using default parameters. Docking was performed with AutoDock 3.05,[2] which predicts the bound conformations of a small, flexible ligand to a nonflexible macromolecular target of known structure (21). This software is an automated docking package that combines a rapid grid-based method for energy evaluation with a Lamarckian genetic algorithm method of conformation search. All of the molecular modeling calculations and manipulations were performed on Silicon Graphics O2 (Silicon Graphics Inc., Mountain View, CA).

Statistical Analysis. Each experiment was performed in triplicate unless otherwise mentioned. All of the experiments were carried out at least twice on different occasions. Where appropriate, the data are presented as the mean + SD.

RESULTS

Structural Optimization of Celecoxib in PDK-1 Inhibition. On the basis of structure-activity analysis, we reported previously a working model that defined structural features essential to the apoptotic effect of celecoxib in PC-3 prostate cancer cells (5). This model suggested that the 5-aryl and sulfonamide ($-SO_2NH_2$) moieties were amenable to alterations, whereas the electrostatic potential surrounding the heterocyclic system was integral to the apoptosis-inducing potency. Accordingly, in the first series of structural modifications, the 4-methylphenyl moiety of celecoxib was replaced by a series of aromatic groups with discrete stereochemical properties, whereas the integrity of the pyrazole ring was maintained. The structure and potency in inhibiting PDK-1 kinase activity and PC-3 cell growth of 24 representative derivatives are summarized in Fig. 1.

These compounds, except the indole derivative 8, showed improved PDK-1 inhibitory and antiproliferative activities vis-à-vis celecoxib, whereas none of these derivatives displayed measurable COX-2 inhibitory activity (data not shown). This finding confirmed the structural divergence required for the inhibition of PDK-1 *versus* COX-2 (5). A general increase in PDK-1 inhibitory activity was noted with increasing bulkiness of the aromatic ring, *i.e.*, tricyclic aromatic rings (21–23) > substituted biphenyl (9–19) > substituted phenyl (1–6). These data, together with the decrease in potency in compound 8, suggested that the aromatic system bound to a large, hydrophobic region of the enzyme pocket. Among the 24 analogs examined, compound 23 (designated as OSU-02067) represented the optimal derivative with IC_{50} values of 9 μM and 5 μM for inhibiting PDK-1 activity and PC-3 cell viability, respectively (Fig. 2, *A* and *C*). These IC_{50} values corresponded to a 5–6-fold improvement over the activities of celecoxib (48 μM and 30 μM, respectively). However, the OSU-02067 isomer 24 exhibited a precipitous decrease in PDK-1 inhibitory activity, which might be attributable to steric hindrance imposed by an unfavorable orientation of the tricyclic aromatic ring.

There existed a correlation between PDK-1 and PC-3 growth inhibition potency in all of the compounds examined, suggesting the mechanistic relevance of PDK-1 inhibition to the antiproliferative effect. Overall, the IC_{50} value for inhibiting PC-3 cell proliferation was approximately one half of that of PDK-1 inhibition. This discrepancy might arise from a mechanistic synergy between PDK-1 inhibition and concomitant Akt dephosphorylation by protein phosphatase 2A in drug-treated cells, resulting in augmented Akt deactivation. To examine this premise, PC-3 cells were treated with different concentrations of OSU-02067 for 2 h, and the consequent effect on Akt was assessed by two independent assays: immunoprecipitated Akt kinase activity (Fig. 2*B*, *top panel*) and Akt phosphorylation status (Fig. 2*B*, *bottom panel*). As shown, both assays gave consistent results.

[1] Internet address: http://www.scripps.edu/pub/olson-web/doc/autodock/tools.html.

[2] Internet address: http://www.scripps.edu/pub/olson-web/people/gmm/autodock/obtaining.html.

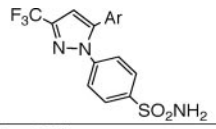

No.	Ar	IC_{50} (μM) PDK-1	PC-3	No.	Ar	IC_{50} (μM) PDK-1	PC-3
Celecoxib	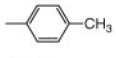	48	30	**13**	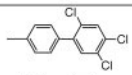	9	5
1	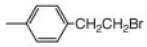	42	18	**14**	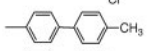	15	8
2	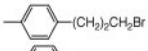	38	17	**15**	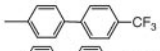	18	8
3	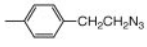	32	17	**16**	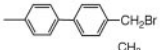	16	8
4	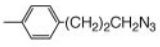	34	18	**17**	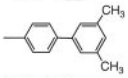	17	9
5	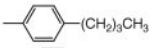	18	9	**18**	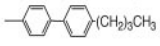	32	15
6	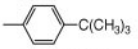	34	18	**19**	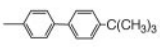	32	15
7		24	11	**20**	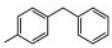	15	8
8		65	31	**21**		16	9
9	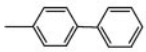	21	11	**22**		12	7
10	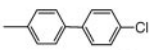	22	9	**23**		9	5
11	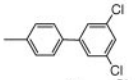	18	10	**24**		42	23
12	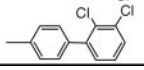	23	10				

Fig. 1. Structures and potency for inhibiting recombinant 3-phosphoinositide-dependent kinase-1 (PDK-1) kinase activity and for inducing apoptotic death in PC-3 cells for celecoxib and derivatives 1–24. The general structure of these compounds is shown at the *top*. Ar represents the respective aromatic ring structures. The reported IC_{50} values are concentrations at which recombinant PDK-1 kinase activity is inhibited by 50% or at which PC-3 cell death measures 50% relative to DMSO control after 24 h-exposure in 1% fetal bovine serum-containing RPMI 1640.

According to the kinase assay, the IC_{50} of OSU-02067 for inhibiting intracellular Akt activation was 5 μM vis-à-vis 28 μM for celecoxib. Neither OSU-02067 nor other celecoxib derivatives displayed a direct inhibitory effect on immunoprecipitated Akt activity. Meanwhile, Western blot analysis shows that treatment of PC-3 cells with OSU- 02067 at ≥5 μM led to significant Akt dephosphorylation.

The inhibition of PDK-1/Akt signaling led to apoptotic death in PC-3 cells in 1% of FBS-containing RPMI 1640 in a dose-dependent manner (Fig. 2*C*), as evidenced by DNA fragmentation (Fig. 2*D*, *top panel*) and PARP cleavage (Fig. 2*D*, *bottom panel*). The dose of OSU-02067 required to induce 50% PC-3 cell death at 24 h was 5 μM, as compared with that of ~30 μM for celecoxib (data not shown). The IC_{50} values for both OSU-02067 and celecoxib to induce PC-3 cell death was consistent with that of inhibiting Akt activation in drug-treated cells. Furthermore, the effect of OSU-02067 vis-à-vis celecoxib on PC-3 cell proliferation was examined in 10% FBS-supplemented RPMI 1640 (Fig. 2*E*). As shown, OSU-02067 at 1 μM showed substantial antiproliferative activity, exceeding that of 30 μM celecoxib. Together, these data clearly indicated the *in vitro* efficacy of OSU-02067 in PC-3 growth inhibition and prompted us to undertake additional lead optimization via structure-based design.

Molecular Modeling and Structure-Based Optimization. Kinetics of PDK-1 inhibition by celecoxib with respect to ATP was examined to shed light onto the mechanistic basis by which these celecoxib derivatives mediated enzyme inhibition. The inhibitory effect of celecoxib on PDK-1 kinase activity was determined in the presence of various concentrations of ATP. Kinetic data revealed an inverse relationship between the degree of celecoxib-exerted PDK-1 inhibition and ATP concentrations. The resulting Lineweaver-Burke plot indicated that celecoxib inhibited PDK-1 through competition with ATP (Fig. 3).

This mode of inhibition (*i.e.*, ATP competition) is common among numerous classes of protein or lipid kinase inhibitors that possess therapeutic potential (22), including those of Bcr-Abl (*e.g.*, Gleevec; Refs. 23–25), epidermal growth factor receptors (*e.g.*, Iressa; Ref. 26), phosphatidylinositol 3′-kinase (*e.g.*, LY294002; Ref. 27), protein kinase C (staurosporine; Ref. 28), cyclin-dependent kinases (29), and vascular endothelial growth factor receptors (30). Structure-activity data indicate that although the ATP-binding site is conserved, architecture in the proximal regions of different protein kinases provides a high degree of diversity (22). Evidence indicates that this diversity allows the design of selective kinase inhibitors.

Together, these findings provided a molecular rationale for structure-based optimization on the basis of the framework generated by the crystal structure of PDK-1-ATP complex (31). OSU-02067 was docked into the ATP-binding domain that is located within a deep cleft between the two lobes of PDK-1 (Fig. 4*A*). Although OSU-02067 competed with ATP for binding, the mode of binding for OSU-02067 was found to be somewhat different from that of ATP (Fig. 4*B*).

Although the benzenesulfonamide moiety occupied the adenine-binding motif, the planar pyrazole moiety was perpendicular to the ribose ring. This arrangement positioned the adjacent phenanthrene ring behind the trisphosphate-binding pocket. The phenanthrene ring formed hydrophobic interactions with an apolar region formed by residues 88–96 encompassing part of two adjacent β sheets joined by a glycine-rich loop. This locality, adjoining to the phosphate-binding motif, could be exploited for structural optimization as demonstrated by the >5-fold increase in potency of OSU-02067 (IC_{50}, 9 μM) over celecoxib (IC_{50}, 48 μM). This hydrophobic cleft appeared to favor the binding of a large, planar aromatic system such as the phenanthrene ring. For example, as compared with OSU-02067, compounds 9–19,

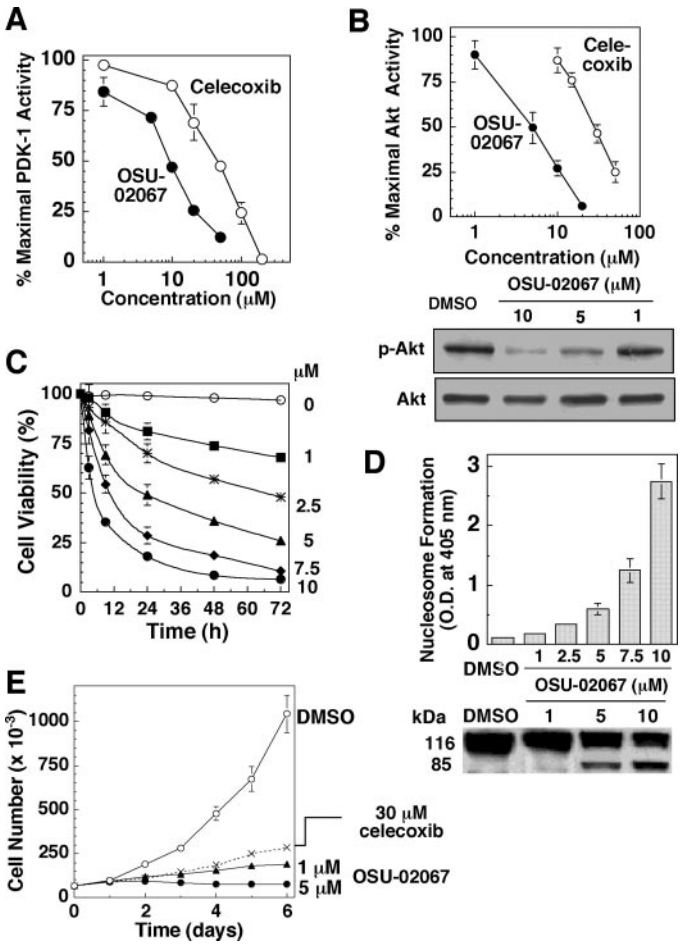

Fig. 2. Effects of OSU-02067 on 3-phosphoinositide-dependent kinase-1 (*PDK-1*) kinase activity, intracellular Akt activation, and survival of PC-3 cells. *A*, dose-dependent inhibition of recombinant PDK-1 kinase activity by OSU-02067 *versus* celecoxib. *B*, *top*, effect of OSU- 02067 *versus* celecoxib on the kinase activity of Akt immunoprecipitated from drug-treated PC-3 cells. *Bottom*, phosphorylation status of Akt in PC-3 cells treated with increasing concentrations of OSU-02067. Control PC-3 cells received DMSO vehicle. *C*, time- and dose-dependent effects of OSU-02067 on the viability of PC-3 cells. Cells were exposed to the indicated concentrations in 1% fetal bovine serum-supplemented RPMI 1640 for different time intervals. Control PC-3 cells received DMSO vehicle. Cell viability was analyzed by the 3-(4,5-dimethylthiazol-2-yl)-2,5-diphenyltetrazolium bromide assay. *D*, evidence of apoptotic death in OSU-02067-treated PC-3 cells. *Top*, formation of cytoplasmic nucleosomal DNA in PC-3 cells treated with DMSO vehicle or the indicated concentrations of OSU-02067. DNA fragmentation was quantitatively measured by a cell death detection ELISA kit. O.D. = absorbance. *Bottom*, induction of poly(ADP-ribose) polymerase cleavage by OSU-02067 in PC-3 cells. Poly-(ADP-ribose) proteolysis to the apoptosis-specific 85-kDa fragment was monitored by Western blotting. *E*, antiproliferative effect of 1 and 5 μM OSU- 02067 *versus* 30 μM celecoxib in PC-3 cells. PC-3 cells were seeded into six-well plates (50,000 cells/well) and exposed to the test agent at the indicated concentration in 10% fetal bovine serum-supplemented RPMI 1640. At different time intervals, cells were harvested, and counted using a Coulter counter. Values were obtained from triplicates for the aforementioned plots except cell viability (*C*) in which the means of six replicates were used; *bars*, ±SD. Western blots shown in *B* and *D* are representatives of three independent experiments.

containing conformationally more flexible biphenyl systems, were less effective in enzyme inhibition. The discrepancy in potency between celecoxib and OSU-02067 was likely attributable to the desolvation of the hydrophobic amino acid residues upon binding of the methylphenyl *versus* phenanthrenyl moiety (29). Assuming that the measured IC_{50} values were proportional to the K_d of the protein-ligand interaction, the relative free energy difference between celecoxib and OSU-02067 was approximately −4 kJ/mol. The upper limit for the free energy associated with the desolvation of hydrophobic groups has been estimated to be −136 J/mol•Å^2 (32). Considering that the binding of the phenanthrene ring of OSU-02067 covers 32 Å^2 more apolar surface than the methylphenyl moiety does, the corresponding free energy change was estimated to be −4.35 kJ/mol, which is consistent with the experimentally measured free energy difference.

The sulfonamide group (either oxygen or nitrogen) formed hydrogen bonds with the backbone amide of Ala162 in the hinge region. This bond lattice mimicked one of the two hydrogen bonds formed by the adenine of ATP in the same microdomain, in which 6-NH donates a hydrogen bond to carbonyl of Ser160 and 1-N accepts a hydrogen bond from NH of Ala162 (31). No hydrogen bond was formed between the pyrazole ring and Glu166, but the ribose of ATP accepts a hydrogen bond from Glu166. In light of the importance of hydrogen bonding with Ala 162 and Ser160 in ligand anchoring, we carried out structure optimization of OSU-02067 by replacing its sulfonamide moiety with a series of heteroatom-rich functional groups that could potentially form hydrogen bonding with the backbone amide and/or carbonyl of these two residues. Structures of 13 representative derivatives, their potency against PDK-1, and their ability to cause apoptotic death in PC-3 cells are summarized in Fig. 5.

Among these derivatives, compounds 34 (designated as OSU-03012) and 35 (designated as OSU-03013) exhibited IC_{50} values for PDK-1 inhibition of 5 and 2 μM, respectively, which represented 2- and 5-fold increases in potency over OSU-02067 (Fig. 6*A*).

Compounds 34 and 35 contained side chains of 2-aminoacetamide and guanidine, respectively. This improvement in potency reflected a strengthening of the hydrogen bonding in the protein-ligand interactions for these derivatives. This premise was supported by the modeled docking of OSU-03013 into the ATP-binding site (Fig. 4*C*). The guanidino group of OSU-03013 resembled the partial structure of the purine ring of ATP, which allowed the formation of hydrogen bonds with Ser160 and Ala162 as depicted by the docking model.

Like OSU-02067, they exhibited no appreciable direct inhibition on immunoprecipitated Akt kinase activity (data not shown) nor was any measurable COX-2 inhibitory activity detected at concentrations up to 50 μM. As shown in Fig. 6*B*, exposure of PC-3 cells to either agent, even at 1 μM, resulted in a substantial decrease in the phospho-Akt level. Because PDK-1 also phosphorylates other members of the AGS protein kinase family such as $p70^{S6K}$ (20, 33–35), we assessed the kinase activity of immunoprecipitated $p70^{S6K}$ in drug-treated PC-3 cells. As indicated in Fig. 6*C*, the activity of immunoprecipitated $p70^{S6K}$ was reduced in a dose-dependent manner after exposing PC-3 cells to OSU-03012 at the indicated concentrations for 6 h.

Cellular Effects of PDK-1/Akt Signaling Inhibitors. Both OSU-03012 and OSU- 03013 induced apoptotic death in PC-3 cells in 1% FBS-containing medium in a dose-dependent manner, as demon-

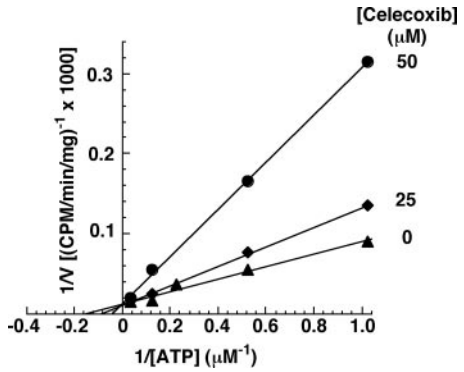

Fig. 3. Lineweaver-Burke plots of the competition of celecoxib with ATP in 3-phosphoinositide-dependent kinase-1 kinase activity. Activity of the recombinant in 3-phosphoinositide-dependent kinase-1 kinase toward the peptide substrate was determined using 1–100 μM ATP in the presence of 0, 25, and 50 μM celecoxib, as described in "Materials and Methods."

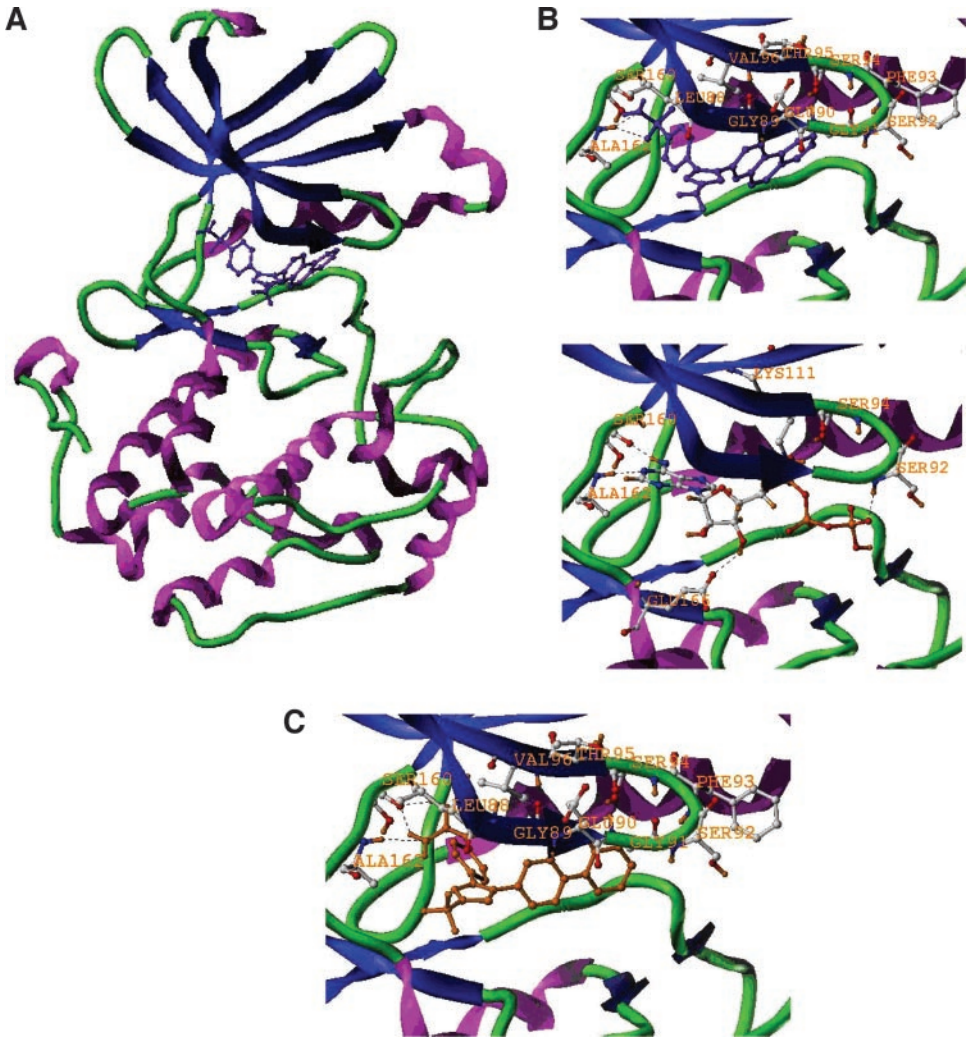

Fig. 4. Modeled docking of various ligands into the ATP-binding site of 3-phosphoinositide-dependent kinase-1. *A*, model of OSU-02067 docked into the ATP-binding domain. OSU-02067 is in *purple*. *B*, comparison of the mode of interactions of OSU-02067 (*top*) and ATP (*bottom*) with the ATP-binding domain. *C*, a model of OSU-03013 docked into the ATP-binding domain. OSU-03013 is in *maroon*.

strated by DNA fragmentation and PARP cleavage (Fig. 7, *A* and *B*). These agents exhibited higher potency than OSU-02067 in apoptosis induction at concentrations >2.5 μM.

The effects of OSU-03012 and OSU-03013 on PC-3 cell proliferation in 10% FBS-supplemented medium were also examined (Fig. 7*C*). High levels of serum might affect the efficacy of these PDK-1 inhibitors due to several factors. First, these celecoxib derivatives might display high serum-binding affinity, thereby sequestering them from entering cells. Second, continuous stimulation of phosphatidylinositol 3′-kinase/Akt signaling through various growth factor receptors counters the inhibitory effect of these agents on Akt. Third, serum could up-regulate Bcl-xL in PC-3 cells, which enhances the threshold to apoptotic signals emanating from phosphatidylinositol 3′-kinase/Akt inhibition (36). As shown, OSU-03012 was effective in suppressing PC-3 cell proliferation at sub-μM, consistent with that noted in 1% serum. In contrast, OSU-03013 required higher concentrations than OSU-03012 to achieve the same degree of antiproliferative effects although it had higher PDK-1 inhibitory potency.

To confirm that inhibition of PDK-1/Akt signaling represented the underlying antitumor mechanism for these agents, we assessed the protective effect of the transient expression of the constitutively active forms of PDK-1 and Akt [PDK-1^{A280V} (37) and $Akt^{T308D/S473D}$ (38), respectively] on the drug-induced PC-3 cell death. Western blot analysis using antibodies against PDK-1, Akt, and the respective myc and hemagglutinin tags confirmed that transient transfection of PDK-1^{A280V} and $Akt^{T308D/S473D}$ into PC-3 cells led to increase in the expression levels of the respective kinases (Fig. 8*A*). These transient transfectants were exposed to 1–10 μM OSU-03012 in 1% FBS-containing medium for 24 h to examine the susceptibility to OSU-03012-induced cell death vis-à-vis transfectants with an empty pcDNA vector. As shown, both PDK-1^{A280V} and $Akt^{T308D/S473D}$ expression gave partial, yet significant, protection against OSU-03012-induced apoptotic death (Fig. 8*B*), which underscores the involvement of both kinases in the antitumor effects of these celecoxib derivatives.

Moreover, these derivatives were submitted to the Developmental Therapeutic Program at the National Cancer Institute for screening against 60 human tumor cell lines, representing leukemia, melanoma, and cancers of the lung, colon, brain, ovary, breast, prostate, and kidney.[3] Dose-response data of one representative cell line from each class of tumor cells after 2-day exposure in 5% FBS-containing medium are shown in Fig. 9, which include: (*a*) RPMI- 8226 leukemia cells; (*b*) NCI-H322M non-small cell lung cancer cells; (*c*) HT29 colon cancer cells; (*d*) U251 glioblastoma cancer cells; (*e*) SK-MEL-28 melanoma cancer cells; (*f*) SK-OV-3 ovarian cancer cells; (*g*) RXF 393 renal cancer cells; (*h*) PC-3 prostate cancer cells; and (*i*) MDA-MB-231 breast cancer cells. Many of these cell lines were responsive to the growth inhibitory effect of both agents at concentrations as low as 0.1 μM.

[3] Internet address: http://dtp.nci.nih.gov/index.html.

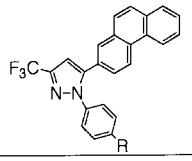

No.	R	IC_{50} (μM) PDK-1	PC-3	No.	R	IC_{50} (μM) PDK-1	PC-3
25	$-CONH_2$	12	7	**32**	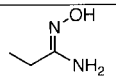	15	8
26	—CN	45	30	**33**	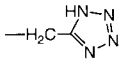	45	27
27		40	25	**34** (**OSU-03012**)	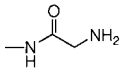	5	5
28		52	32	**35** (**OSU-03013**)	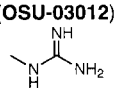	2	3
29		25	14	**36**	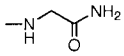	14	8
30	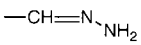	16	10	**37**	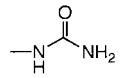	40	24
31	$-CH_2CN$	42	25				

Fig. 5. Structures and potency for inhibiting recombinant 3-phosphoinositide-dependent kinase-1 (*PDK-1*) kinase activity and for inducing apoptotic death in PC-3 cells for derivatives 25–37. The general structure of these compounds is shown at the *top*. R represents the respective substitution in place of the sulfonamide moiety. The reported IC_{50} values are concentrations at which PDK-1 kinase activity is inhibited by 50% or at which PC-3 cell death measures 50% relative to DMSO control after 24 h-exposure in 1% fetal bovine serum-containing RPMI 1640.

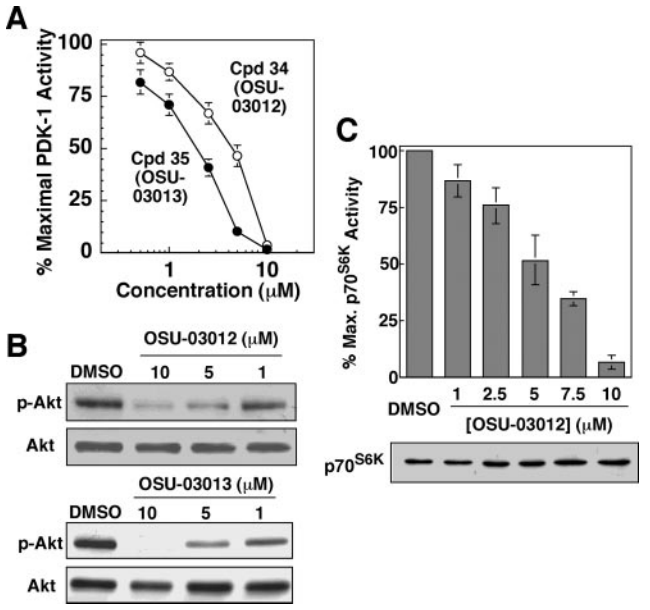

Fig. 6. Effects of OSU-03012 and OSU-03013 on recombinant 3-phosphoinositide-dependent kinase-1 (*PDK-1*) kinase activity and intracellular Akt activation in drug-treated PC-3 cells. *A*, dose-dependent inhibition of recombinant PDK-1 kinase activity by OSU-03012 and OSU-03013. Values were obtained from three replicates; *bars*, ±SD. *B*, effect of OSU-03012 (*top*) and OSU-03013 (*bottom*) on the phosphorylation status of Akt in drug-treated PC-3 cells. PC-3 cells were seeded in T-25 flasks at the density of 4×10^5 cells/flask, incubated in 10% fetal bovine serum-supplemented RPMI 1640 for 24 h, and exposed to the test agent at the indicated concentrations in 1% fetal bovine serum-supplemented medium for 6 h. Control PC-3 cells received DMSO vehicle. Western blots are representatives of three independent experiments. *C*, effect of OSU-03012 on the kinase activity of immunoprecipitated p70 S6 kinase ($p70^{S6K}$) in drug-treated PC-3 cells. PC-3 cells were seeded in T-75 flasks at the density of 1.5×10^6 cells/flask, allowed to attach for 24 h, and treated with OSU-03012 for 6 h. $p70^{S6K}$ was immunoprecipitated from equal amounts of total protein, and the kinase activity was analyzed as described in "'Materials and Methods" (*top*). Values are means; *bars*, ±SD ($n = 3$). A portion of the cell lysates was separated by SDS-PAGE and Western blotted using antibodies specific for $p70^{S6K}$ (*bottom*).

In the 60 cell line assay, three dose-response parameters for each cell line were calculated based on growth inhibition curves. These parameters include concentration resulting in 50% growth inhibition, concentration resulting in total growth inhibition, and concentration resulting in a 50% reduction in the measured protein level at the end of drug treatment as compared with that at the beginning. The means of these parameters among the 60 different cell lines for OSU-03012 and OSU-03013 after 2-day treatment were as follows, respectively, concentration resulting in 50% growth inhibition, 1.1 and 1.2 μM; concentration resulting in total growth inhibition, 3.2 and 2.9 μM; and concentration resulting in a 50% reduction in the measured protein level at the end of drug treatment as compared with that at the beginning, 6.8 and 8.5 μM. In contrast, for OSU-02067, the corresponding values were 3.0, 19, and 66 μM, respectively. These data clearly demonstrate the *in vitro* efficacy of OSU-03012 and OSU-03013. Both agents were able to completely suppress cell growth in a diverse range of tumor cell lines at the 3–5 μM therapeutic range, as compared with the concentration of at least 50 μM required for celecoxib.

DISCUSSION

In light of the conserved role of PDK-1/Akt signaling in cancer cell survival and proliferation (9, 10, 12–15), this pathway represents a therapeutically relevant target for developing orally bioavailable, small-molecule inhibitors. Our previous structure-activity analysis provided a proof of principle that the apoptosis-inducing activity of celecoxib could be separated from its COX-2 inhibitory activity via structural modifications (5). Furthermore, these data allowed us to establish a working model depicting the structural attributes essential to the PDK-1 *versus* COX-2 inhibitory activity of celecoxib. This model, in conjunction with the crystal structure of PDK-1-ATP complexes reported recently (31), provided a molecular foundation for the present structure-based optimization. Kinetic and molecular modeling data indicate that celecoxib derivatives exerted PDK-1 inhibition by competing with ATP for binding, a mechanism shared by many types

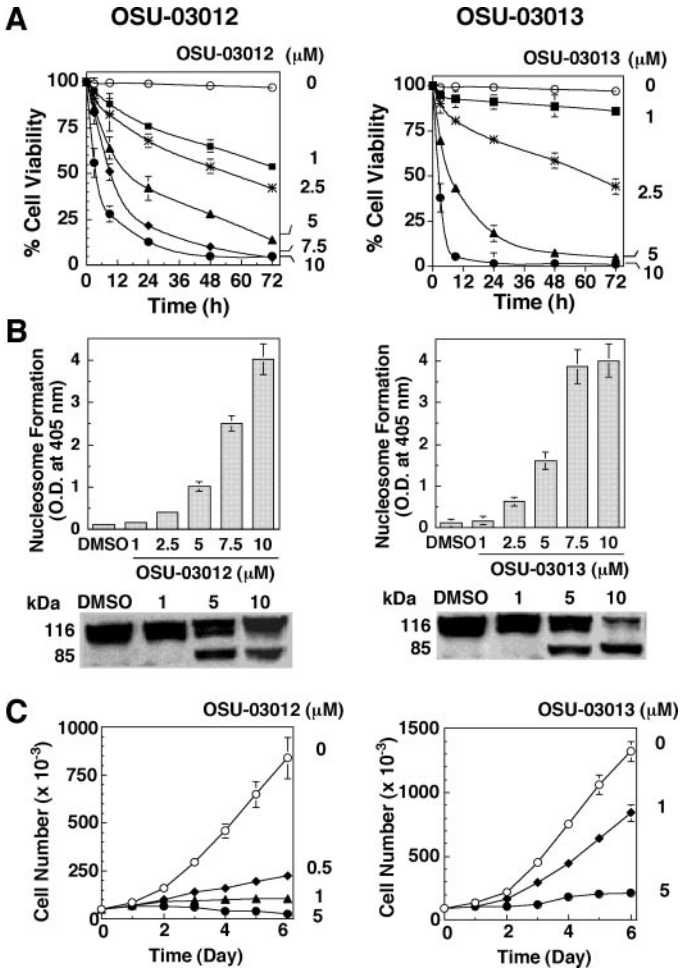

Fig. 7. Dose-dependent effects of OSU-03012 (*left*) and 03013 (*right*) on cell viability of PC-3 cells. *A*, time- and dose-dependent effects of OSU-03012 (*left*) and OSU-03013 (*right*) on the viability of PC-3 cells. Cells were exposed to the indicated concentrations of the test agent in 1% fetal bovine serum-supplemented RPMI 1640 for different time intervals. Control PC-3 cells received DMSO vehicle. Cell viability was analyzed via 3-(4,5-dimethylthiazol-2-yl)-2,5-diphenyltetrazolium bromide assay. *B*, evidence of apoptotic death in drug-treated PC-3 cells. *Top*, formation of cytoplasmic nucleosomal DNA in PC-3 cells treated with DMSO vehicle or the indicated concentrations of OSU-03012 (*left*) or 03013 (*right*). DNA fragmentation was quantitatively measured by a cell death detection ELISA kit. O.D. = absorbance. *Bottom*, induction of poly(ADP-ribose) polymerase cleavage by OSU-03012 (*left*) or 03013 (*right*) in PC-3 cells as measured by immunoblotting. Western blots are representatives of three independent experiments. *C*, antiproliferative effect of OSU-03012 (*left*) and OSU- 03013 (*right*) in PC-3 cells. PC-3 cells were seeded into six-well plates at ~75,000 cells/flask and exposed to the test agent at the indicated concentration in 10% fetal bovine serum-supplemented RPMI 1640. At different time intervals, cells were harvested and counted using a Coulter counter. Data represent means; *bars*, ±SD ($n = 6$).

of kinase inhibitors. Structural optimization of celecoxib by altering the terminal phenyl ring led to OSU-02067 with a 5-fold improvement in PDK-1 inhibitory potency. This improvement was attributable to enhanced hydrophobic ligand interactions with the apolar region adjacent to the trisphosphate-binding pocket. Moreover, *in silico* docking of OSU-02067 into the ATP-binding pocket showed that the molecule was anchored into the ATP binding domain, in part, through hydrogen bonding between the sulfonamide and the amide of Ala162. Ala162 has also been reported to play a key role in anchoring other ligands such as ATP (31) and UCN-01 (39) to PDK-1. Together, these data suggest that the sulfonamide moiety of OSU-02067 might be amenable to alterations for optimizing potency.

Accordingly, replacement of the sulfonamide function with 2-aminoacetamide and guanidine led to OSU-03012 and OSU-03013, respectively, both of which exhibited improved PDK-1 inhibition with IC_{50} values of 5 and 2 μM, respectively (Fig. 6*A*). Docking of OSU-03013 into the ATP binding site revealed increased hydrogen bonding between the guanidine moiety and the backbone oxygen of Ser160. The effect of these substituents on ligand binding, however, was subtle, as illustrated by the structure-activity relationship summarized in Fig. 5.

The high potency of OSU-03012 and OSU-03013 in PDK-1 inhibition was reflected in their abilities to effectively block the activation of Akt and $p70^{S6K}$ (Fig. 6) and to induce apoptotic cell death in PC-3 cells at low μM concentrations (Fig. 7). More importantly, due to the conserved role of PDK-1/Akt signaling in cell proliferation and survival, these agents were potent in inhibiting cell growth in serum-containing medium in all 60 of the human tumor cell lines examined, with mean concentration resulting in 50% growth inhibition values of 1.2 μM and 1.3 μM, respec-

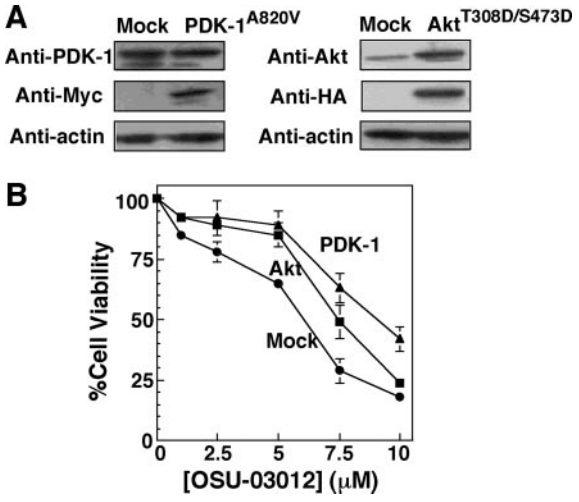

Fig. 8. Protective effect of constitutively active 3-phosphoinositide-dependent kinase-1 (*PDK-1*) and Akt on OSU-03012-induced apoptotic death in PC-3 cells. *A*, expression of $Akt^{T308D/S473D}$ (*left*) PDK-1^{A820V} (*right*) in PC-3 transient transfections. Western blot analysis used antibodies against PDK-1, Akt, and the respective myc and hemagglutinin (*HA*) tags. *B*, viability of PC-3 cells overexpressing $Akt^{T308D/S473D}$ or PDK-1^{A820V} vis-à-vis cells transfected with empty pcDNA vector (*mock*) in the presence of the indicated amount of OSU-03012 in 1% fetal bovine serum-supplemented medium for 24 h. Values are means; *bars*, ±SD ($n = 3$).

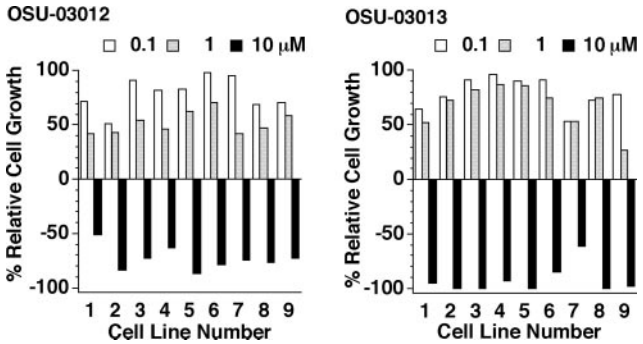

Fig. 9. Growth inhibitory effect of OSU-03012 (*left*) and OSU-03013 (*right*) on 9 representative human tumor cell lines from a panel of 60 cell lines. This screening service was provided by the Developmental Therapeutics Program at National Cancer Institute. These 9 cell lines are *1*, RPMI-8226 leukemia cells; *2*, NCIH322M non-small cell lung cancer cells; *3*, HT29 colon cancer cells; *4*, U251 glioblastoma cancer cells; *5*, SK-MEL-28 melanoma cancer cells; *6*, SK-OV-3 ovarian cancer cells; *7*, RXF 393 renal cancer cells; *8*, PC-3 prostate cancer cells; and *9*, MDA-MB-231 breast cancer cells. A sulforhodamine B (SRB) protein assay was used to estimate cell viability or growth. The relative cell growth (PG) was calculated according to the following equation: $PG = 100 \times [(\text{Mean } OD_{Test} - \text{Mean } OD_{T=0})/(\text{Mean } OD_{Control} - \text{Mean } OD_{T=0})$, in which Mean $OD_{T=0}$ represents the average of absorbance measurements of SRB-derived color just before exposure of cells to the test compound; Mean OD_{Test} denotes the average of absorbance measurements of SRB-derived color after 48-h exposure of cells to the test compound; Mean $OD_{Control}$ is the average of absorbance measurements of SRB-derived color after 48 h with no exposure of cells to the test compound.

tively, and concentration resulting in total growth inhibition (total growth inhibition) values of 3.2 and 2.9 μM, respectively.

In summary, the present study has clearly demonstrated the successful development of a new class of PDK-1/Akt signaling inhibitors via structure-based optimization of celecoxib. In light of the prominent role of PDK-1/Akt signaling in different stages of tumorigenesis, these molecules have translational potential to be developed into antitumor agents for the prevention and/or therapy of cancers alone or in combination with other treatments. Testing of *in vivo* efficacy against different tumor xenografts in nude mice is currently under way in this laboratory.

ACKNOWLEDGMENTS

We thank Drs. Rao Vishnuvajjala and Robert Schultz in the Developmental Therapeutics Program at National Cancer Institute for critical comments on this manuscript. The *in vitro* 60-cell line screening was carried out by the Developmental Therapeutic Program anticancer drug discovery program.

REFERENCES

1. Steinbach G, Lynch PM, Phillips RK, et al. The effect of celecoxib, a cyclooxygenase-2 inhibitor, in familial adenomatous polyposis. N Engl J Med 2000;342:1946–52.
2. Hsu AL, Ching TT, Wang DS, Song X, Rangnekar VM, Chen CS. The cyclooxygenase-2 inhibitor celecoxib induces apoptosis by blocking Akt activation in human prostate cancer cells independently of Bcl-2. J Biol Chem 2000;275:11397–403.
3. Johnson AJ, Song X, Hsu A, Chen C. Apoptosis signaling pathways mediated by cyclooxygenase-2 inhibitors in prostate cancer cells. Adv Enzyme Regul 2001;41: 221–35.
4. Song X, Lin HP, Johnson AJ, et al. Cyclooxygenase-2, player or spectator in cyclooxygenase-2 inhibitor-induced apoptosis in prostate cancer cells. J Natl Cancer Inst 2002;94:585–91.
5. Zhu J, Song X, Lin HP, Young DC, Yan S, Marquez VE, Chen CS. Using cyclooxygenase-2 inhibitors as molecular platforms to develop a new class of apoptosis-inducing agents. J Natl Cancer Inst 2002;94:1745–57.
6. Grosch S, Tegeder I, Niederberger E, Brautigam L, Geisslinger G. COX-2 independent induction of cell cycle arrest and apoptosis in colon cancer cells by the selective COX-2 inhibitor celecoxib. FASEB J 2001;15:2742–4.
7. Arico S, Pattingre S, Bauvy C, et al. Celecoxib induces apoptosis by inhibiting 3-phosphoinositide-dependent protein kinase-1 activity in the human colon cancer HT-29 cell line. J Biol Chem 2002;277:27613–21.
8. Kulp SK, Yang YT, Hung CC, et al. PDK-1/Akt signaling represents a major COX-2-independent target for celecoxib in prostate cancer cells. Cancer Res 2004;64:1444–51.
9. Datta SR, Brunet A, Greenberg ME. Cellular survival: a play in three Akts. Genes Dev 1999;13:2905–27.
10. Chan TO, Rittenhouse SE, Tsichlis PN. AKT/PKB and other D3 phosphoinositide-regulated kinases: kinase activation by phosphoinositide-dependent phosphorylation. Annu Rev Biochem 1999;68:965–1014.
11. Roymans D, Slegers H. Phosphatidylinositol 3-kinases in tumor progression. Eur J Biochem 2001;268:487–98.
12. Toker A, Newton AC. Cellular signaling: pivoting around PDK-1. Cell 2000;103:185–8.
13. Storz P, Toker A. 3′-phosphoinositide-dependent kinase-1 (PDK-1) in PI 3- kinase signaling. Front Biosci 2002;7:d886–902.
14. Vivanco I, Sawyers CL. The phosphatidylinositol 3-Kinase AKT pathway in human cancer. Nat Rev Cancer 2002;2:489–501.
15. Cantley LC. The phosphoinositide 3-kinase pathway. Science 2002;296:1655–7.
16. Di Cristofano A, Pandolfi PP. The multiple roles of PTEN in tumor suppression. Cell 2000;100:387–90.
17. Downes CP, Bennett D, McConnachie G, et al. Antagonism of PI 3-kinase-dependent signalling pathways by the tumour suppressor protein, PTEN. Biochem Soc Trans 2001;29:846–51.
18. Leslie NR, Downes CP. PTEN: The down side of PI 3-kinase signalling. Cell Signalling 2002;14:285–95.
19. Waite KA, Eng C. Protean PTEN: form and function. Am J Hum Genet 2002;70:829–44.
20. Flynn P, Wongdagger M, Zavar M, Dean NM, Stokoe D. Inhibition of PDK-1 activity causes a reduction in cell proliferation and survival. Curr Biol 2000;10:1439–42.
21. Morris GM, Goodsell DS, Halliday RS, et al. Automated docking using a Lamarckian genetic algorithm and empirical binding free energy function. J Comput Chem 1998;19:1639–62.
22. Fabbro D, Ruetz S, Buchdunger E, et al. Protein kinases as targets for anticancer agents: from inhibitors to useful drugs. Pharmacol Ther 2002;93:79–98.
23. Druker BJ, Tamura S, Buchdunger E, et al. Effects of a selective inhibitor of the Abl tyrosine kinase on the growth of Bcr-Abl positive cells. Nat Med 1996;2:561–6.
24. Buchdunger E, Zimmermann J, Mett H, et al. Inhibition of the Abl protein-tyrosine kinase in vitro and in vivo by a 2- phenylaminopyrimidine derivative. Cancer Res 1996;56:100–4.
25. Deininger MW, Goldman JM, Lydon N, Melo JV. The tyrosine kinase inhibitor CGP57148B selectively inhibits the growth of BCR-ABL-positive cells. Blood 1997; 90:3691–8.
26. Ciardiello F. Epidermal growth factor receptor tyrosine kinase inhibitors as anticancer agents. Drugs 2000;60(Suppl 1): 25–32; discussion 41–22.
27. Vlahos CJ, Matter WF, Hui KY, Brown RF. A specific inhibitor of phosphatidylinositol 3-kinase, 2-(4-morpholinyl)-8-phenyl-4H-1-benzopyran-4-one (LY294002). J Biol Chem 1994;269:5241–8.
28. Prade L, Engh RA, Girod A, Kinzel V, Huber R, Bossemeyer D. Staurosporine-induced conformational changes of cAMP-dependent protein kinase catalytic subunit explain inhibitory potential. Structure 1997;5:1627–37.
29. Davies TG, Bentley J, Arris CE, et al. Structure-based design of a potent purine-based cyclin-dependent kinase inhibitor. Nat Struct Biol 2002;9:745–9.
30. Hennequin LF, Stokes ES, Thomas AP, et al. Novel 4- anilinoquinazolines with C-7 basic side chains: design and structure activity relationship of a series of potent, orally active, VEGF receptor tyrosine kinase inhibitors. J Med Chem 2002;45:1300–12.
31. Biondi RM, Komander D, Thomas CC, et al. High resolution crystal structure of the human PDK1 catalytic domain defines the regulatory phosphopeptide docking site. EMBO J 2002;21:4219–28.
32. Juffer AH, Eisenhaber F, Hubbard SJ, Walther D, Argos P. Comparison of atomic solvation parametric sets: applicability and limitations in protein folding and binding. Protein Sci 1995;4:2499–509.
33. Pullen N, Dennis PB, Andjelkovic M, et al. Phosphorylation and activation of p70s6k by PDK1. Science 1998;279:707–10.
34. Martin KA, Schalm SS, Richardson C, Romanelli A, Keon KL, Blenis J. Regulation of ribosomal S6 kinase 2 by effectors of the phosphoinositide 3-kinase pathway. J Biol Chem 2001;276:7884–91.
35. Gonzalez-Garcia A, Garrido E, Hernandez C, et al. A new role for the p85-phosphatidylinositol 3- kinase regulatory subunit linking FRAP to p70 S6 kinase activation. J Biol Chem 2002;277:1500–8.
36. Yang CC, Lin HP, Chen CS, Yang YT, Tseng PH, Rangnekar VM. Bcl-xL mediates a survival mechanism independent of the phosphoinositide 3- kinase/Akt pathway in prostate cancer cells. J Biol Chem 2003;278:25872–8.
37. Wick MJ, Dong LQ, Riojas RA, Ramos FJ, Liu F. Mechanism of phosphorylation of protein kinase B/Akt by a constitutively active 3- phosphoinositide-dependent protein kinase-1. J Biol Chem 2000;275:40400–6.
38. Meier R, Thelen M, Hemmings BA. Inactivation and dephosphorylation of protein kinase Balpha (PKBalpha) promoted by hyperosmotic stress. EMBO J 1998;17:7294–303.
39. Komander D, Kular GS, Bain J, Elliott M, Alessi DR, Van Aalten DM. Structural basis for UCN-01 specificity and PDK1 inhibition. Biochem. J. 2003:255–62.

From the Cyclooxygenase-2 Inhibitor Celecoxib to a Novel Class of 3-Phosphoinositide-Dependent Protein Kinase-1 Inhibitors

Jiuxiang Zhu, Jui-Wen Huang, Ping-Hui Tseng, et al.

Cancer Res 2004;64:4309-4318.